Int. J. of Applied Mechanics and Engineering, 2006, vol.11, No.4, pp.735-749

This paper was prepared on the Fourth International Tribology Conference ITC 2006

EVALUATION OF NUMERICAL MODELS FOR PREDICTION OF AREAS SUBJECTED TO EROSION WEAR

B. DOBROWOLSKI and J. WYDRYCH*
Opole University of Technology
Chair of Thermal Engineering and Industrial Apparatus
ul. Mikołajczyka 5, 45-271 Opole, POLAND
e-mail: bolo@po.opole.pl; jacek@po.opole.pl

The paper compares different erosion models. The calculations were carried out in a selected flow system, and results were compared with experimental results of this system. The motion of gas phase was described by Reynolds equations and the particle trajectory was calculated by using Lagrange's method. The simplifications and the different ranges of models' application do not allows us to state which model assures correct results in complicated conditions of flow. For that reason was performed research for a part of the dust system in BP-1150 boiler.

Key words: erosion wear,gas-solid mixture movement, particle trajectory, CFD.

1. Introduction

Dust systems of power boilers, being pneumatic conveying installations, can be subjected to progressive erosion wear. Elements of such dust systems are made of materials resistant to progressive erosion wear, but their life is strictly limited.

The paper presents some models for erosion wear evaluation for pairs of materials: steel/cast iron – sand/coal dust. The presented models were subjected to parametric tests and the calculation results were compared with the results of tests on erosion wear in steel-sand pair. The results of both parametric tests and comparison with empirical data showed a large scatter of the predicted erosion rate. Moreover, it was found that parameters of the particles during their collision with the wall strongly influenced the erosion process. It was proved by the parametric test results for various rates and angles of collisions with the wall. Thus, the possibility of accelerated erosion of particular installation elements is dependent on the aerodynamics of the gas-particles flow. Material constants of the erodent-wall pair influence the wear mechanism and its intensity. The assumed simplifications and different applicability ranges of particular models do not allow to state which model can give correct results under complex flow conditions. Thus, the authors performed their own tests for a real dust installation of the power boiler. The chosen Bitter model allowed to obtain the best results. The paper gives a comparison of the results obtained with different erosion models and the test results.

2. Methods of numerical calculations for the gas-solid mixture movement

For the purpose of numerical tests, the authors applied a mathematical model containing equations of motion for the gaseous phase and the coal dust particles. The air movement was described with the Euler method, for description of the particle motion the Lagrange method was used (Wydrych, 2002).

Because of the possibility of analysing polydispersive gas-particles mixture motion, the PSICell method was used. Phase changes were neglected and it was assumed that both phases were microscopically incompressible, the flow was isothermal and steady, the gas motion could be expressed in a generalized

* To whom correspondence should be addressed

uniform conservative form, where convective, diffusive and source elements could be distinguished. As a result, we obtained the equation

$$\frac{\partial(ru_i f)}{\partial x_i} = \frac{\partial}{\partial x_i}\left(\Gamma_f \frac{\partial f}{\partial x_i}\right) + S_f + S_{fp} \tag{2.1}$$

where ϕ was a generalized dependent variable, Γ_ϕ was the coefficient of diffusive transport, the source term S_ϕ included all the remaining elements of differential equations, excepting convective and diffusive ones. Coefficients Γ_ϕ are S_ϕ are dependent on the variable ϕ and they are determined for each equation according to Tab.1. In the PSICell method it is assumed that particles of the disintegrated phase are sources of mass, momentum and energy, occurring as additional elements $S_{\phi p}$ in continuous (gaseous) phase equations.

Table 1. Coefficients of Eq.(2.1).

Equation of	ϕ	Γ_ϕ	S_ϕ	$S_{\phi p}$
continuity	*1*	*0*	*0*	*0*
momentum in direction of axis x_i	u_i	μ_{ef}	$F_i - \frac{\partial p}{\partial x_i} + \frac{\partial}{\partial x_j}\left(\mu_{ef}\frac{\partial u_j}{\partial x_i}\right)$	$\overline{S_{u_i,p}}$
kinetic energy of turbulence	k	$\frac{\mu_{ef}}{\sigma_k}$	$G_k - \rho\varepsilon$	*0*
dissipation of kinetic energy of turbulence	ε	$\frac{\mu_{ef}}{\sigma_\varepsilon}$	$\frac{\varepsilon}{k}(C_1 G_k - C_2\rho\varepsilon)$	*0*

$$G_k = \frac{\partial u_i}{\partial x_j}\mu_t\left(\frac{\partial u_i}{\partial x_j} + \frac{\partial u_j}{\partial x_i}\right); \quad \mu_{ef} = \mu + \mu_t; \quad \mu_t = C_\mu \rho \frac{k^2}{\varepsilon}$$

$$\overline{S_{u_i,p}} = \frac{1}{V_E}\eta_j \int_{\delta t_j} \frac{\mu C_D \mathrm{Re}_p D_p}{8\pi}\left(\bar{u}_i - u_{pi}\right)dt$$

$$C_\mu = 0.09;\ C_1 = 1.44;\ C_2 = 1.92;\ \sigma_k = 1.0;\ \sigma_e = 1.3$$

Boundary conditions, suitable for all the variables, are joined to the system of equations. The above system of differential equations is nonlinear. The particular equations are conjugate, so special numerical techniques should be used for solving them (FLUENT INC.).

For calculations of source elements $S_{\phi p}$ we must know particle trajectories. A particle trajectory is calculated according to the equation of particle motion (Wydrych, 2002). If the difference between the phase densities is high, the equation of particle motion can be written as

$$m_p \frac{du_p}{dt} = \frac{3}{4} C_D \frac{\rho m_P}{\rho_p dp}\left|u - u_p\right|\left(u - u_p\right) + g \tag{2.2}$$

where m_P is the particle mass, and C_D means the aerodynamic drag coefficient, dependent on the Reynolds number related to the particle diameter and the slide rate

$$\mathrm{Re}_p = \frac{d_p \left| \boldsymbol{u} - \boldsymbol{u}_p \right|}{\nu} \tag{2.3}$$

where
$$\left| \boldsymbol{u} - \boldsymbol{u}_p \right| = \sqrt{\left(u - u_p\right)^2 + \left(v - v_p\right)^2 + \left(w - w_p\right)^2} \,. \tag{2.4}$$

If $\mathrm{Re}_p \le 1$, C_D can be calculated from the Stokes equation

$$C_{Dr} = \frac{24}{\mathrm{Re}_p}. \tag{2.5}$$

For higher Re_p, the empirical correction f is usually introduced, and then

$$C_{Dr} = \frac{24}{\mathrm{Re}_p} f \,. \tag{2.6}$$

In Shuh *et al*. (1989), the following equation was proposed in order to calculate function f

$$f = \begin{cases} 1 + 0.15\,\mathrm{Re}_p^{0.687} & 0 < \mathrm{Re}_p \le 200 \\ 0.914\,\mathrm{Re}_p^{0.282} + 0.0135\,\mathrm{Re}_p & 200 < \mathrm{Re}_p \le 2500 \\ 0.0167\,\mathrm{Re}_p & \mathrm{Re}_p > 2500 \end{cases}. \tag{2.7}$$

The case when a particle collides with a solid wall should be understood as a special one. In such a case, we calculate components of the particle rate vector after the collision in two directions: tangent and normal to the wall surface. It is necessary to know coefficients of restitution, strongly dependent on the coefficient of kinetic friction, the glancing angle, properties of the particle and wall materials, smoothness of the wall surface and the particle shape (Schuh *et al*., 1989).

3. Comparison of the erosion wear models

There are many known methods of erosion rate calculations. Thus, a parametric analysis of some chosen models was performed. Six models were chosen for further consideration. All the considered models of erosion are functions of the glancing angle between the particle and the wall and functions of the particle rate. From among the chosen models, two are based on theoretical derivations for the cutting grain. The remaining four models are empirical. The empirical constants are determined for actual pairs of materials, so extension of these models for other pairs of materials is difficult or even impossible. Table 2 contains the models used for the parametric analysis.

The erosion models were compared according to the known test results for horizontal erosion of the channel wall, being a result of impact of quartz particles (Sato *et al*., 1995). Figure 1 presents the applied test system.

Table 2. Models of erosion wear.

Model No.	Equations describing the model	Constants of the model	Pair of materials wall – erodent
Model I (Finnie, 1960)	$V_{er}=\frac{m_p u_p^2}{w_y k_s e}\frac{w_y}{6}\cos^2\alpha=\frac{m_p u_p^2}{6k_s e}\cos^2\alpha$ $V_{er}=\frac{m_p u_p^2}{w_y k_s e}\left(\sin 2\alpha-\frac{6}{w_y}\sin^2\alpha\right)$	$e=1.4$	steel St4 – sand $k_s=700[MPa]$
Model II (Jun Yong-Du and Tabakoff, 1992)	$er=278{,}90\left[\left(\frac{u_p}{100}\right)^{2{,}47}\cos^2\alpha\left(1-e_t^2\right)+0{,}0832\left(\frac{u_p}{100}\right)^{2{,}344}\sin^2\alpha\left(1-e_n^2\right)\right]$		Steel 410 – high silica sand
Model III (Bitter, 1963)	$M_c=\frac{\rho_t C m_p u_p^2}{P\psi}\left[\sin 2\alpha-\frac{2\left(1+\frac{m_p r_p^2}{I_p}\right)}{w_y}\sin^2\alpha\right]$ $M_c=\frac{\rho_t C m_p u_p^2}{P\psi}\left[\frac{w_y\cos^2\alpha}{2\left(1+\frac{m_p r_p^2}{I_p}\right)}\right]$ $P=\left[\frac{40}{\pi^4}\rho_p\left(\frac{1-q_p^2}{E_p}+\frac{1-q_t^2}{E_t}\right)^{-4}\right]^{1/5}\left(u_p\sin\alpha\right)^{2/5}$ $M_d=\frac{\frac{1}{2}\rho_p m_p\left(u_p\sin\alpha-u_0\right)^2}{\varepsilon_0}$	$w_y=6$ $C=0.015$	Steel St4– sand $\rho_t=7200[kg/m^3]$ $\psi=2$ $\varepsilon_0=700e9[J/m^3]$ $Y=250e6[J/m^2]$ $q_t=0.25$ $E_t=100e9[N/m^2]$ $\rho_p=1600e9\,kg/m^3$ $q_p=0.17$ $E_p=20e9[N/m^2]$
Model IV (Grant and Tabakoff, 1973)	$er=K_A f(\alpha)(u_p\cos\alpha)^2(1-R_T^2)+f(V_{IN})$ $R_T=1-0.0016\,u_p\sin\alpha$ $f(\alpha)=\{1+CK[K_B\alpha\sin(90/\alpha_0)]\}^2$ $f(V_{IN})=K_C(u_p\sin\alpha)^4$	$CK=1(\alpha<3\alpha_0)$ $CK=0(\alpha\geq 3\alpha_0)$ $K_A=3.67\cdot 10^{-6}$ $K_B=0.585$ $K_C=6.0\cdot 10^{-12}$	Steel 355 – high-silica sand
Model V (McLaury *et al.*, 1996)	$er=A\cdot u_p^n\cdot f(\alpha)$ $f(\alpha)=b\cdot\alpha^2+c\cdot\alpha \quad (\alpha\leq\alpha_0)$ $f(\alpha)=x\cdot\cos^2\alpha\cdot\sin(w\alpha)+y\cdot\sin^2\alpha+z \quad (\alpha>\alpha_0)$	$A=1559\,BH^{-0.59}$ $\alpha_0=15^0$ $b=-3.84\cdot 10^{-8}$ $c=2.27\cdot 10^{-8}$ $n=1.73$	Carbon steel – high-silica sand

		$w = 1$ $x = 3.147 \cdot 10^{-9}$ $y = 3.609 \cdot 10^{-10}$ $z = 2.532 \cdot 10^{-9}$	
Model VI (Menguturk and Sverdrup, 1979)	$er_v = 0.00000163 \left(u_p \cos\alpha\right)^{2.5} \sin\left(\frac{\pi\alpha}{45.4^0}\right) + 0.000000468 \left(u_p \sin\alpha\right)^{2.5} \quad \left(\alpha \le 22.7^0\right)$ $er_v = 0.00000163\left(u_p \cos\alpha\right)^{2.5} + 0.000000468\left(u_p \sin\alpha\right)^{2.5} \quad \left(\alpha > 22.7^0\right)$		Carbon steel – coal dust

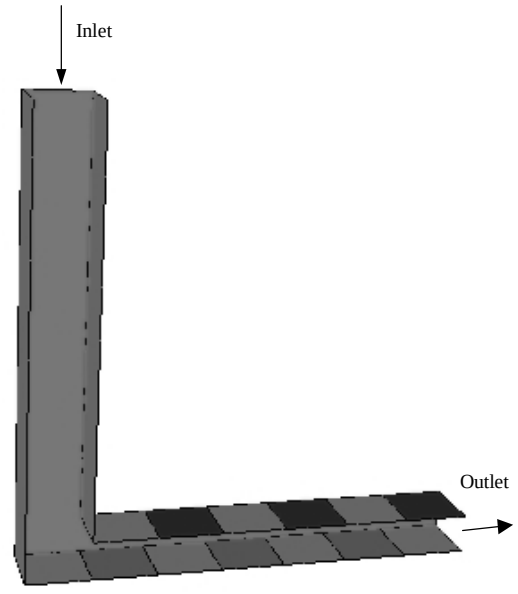

Fig.1. Flow system applied for tests of erosion loss in the walls.

In the experiments (Sato *et al.*, 1995), the inlet part of the channel of the section $50 \times 50\,mm$ was $354mm$ in length, the outlet part had the section $30 \times 50\,mm$ and length $350mm$. The outlet part made of stainless steel segments rendered it possible to perform weight analysis of loss in particular intervals of the channel. The front and back walls of the system were made of transparent acrylic resin, so it was possible to observe the behaviour of erodent particles, especially to measure of the particle glancing angle. The tests were performed for the following mixture rates at the inlet: $9.97\,m/s$, $17.3\,m/s$ and $23.0\,m/s$. A high-silica sand with particles $60\,\mu m$ in diameter was an abrasive factor. Our own programs were used for calculations. The gaseous phase motion in the system under consideration was calculated according to Eq.(2.1). The gas velocity field was applied for the calculation of the trajectory of particles delivered to the system at the inlet section according to Eq.(2.2). The results of three series of tests are presented below. The tests were performed for different velocities and glancing angles. Here you can also find the calculation results obtained with

different methods. In Tables 3-5, wear values are given for different glancing angles and three inlet velocities of the mixture (Sato *et al.*, 1995). In Figures 2-7, erosion wear obtained from the tests is compared with the results of numerical calculations for the same initial conditions.

Table 3. Erosion wear under different particle glancing angles for the particle velocity $9.97\,m/s$ obtained from the tests.

Glancing angle	*15*	*20*	*25*	*30*	*45*	*60*	*75*	*90*
Wear $[mg/kg]$	*1.125*	*1.375*	*1.39*	*1.33*	*0.75*	*0.71*	*0.58*	*0.625*

Table 4. Erosion wear under different particle glancing angles for particle velocity $17\,m/s$ obtained from experiments.

Glancing angle	*15*	*20*	*25*	*30*	*45*	*60*	*75*	*90*
Wear $[mg/kg]$	*2.9*	*2.8*	*3.5*	*3.5*	*3*	*1.15*	*1.2*	*1.05*

Table 5. Erosion wear under different glancing angles for particle velocity $23\,m/s$ obtained from experiments.

Glancing angle	*15*	*20*	*25*	*30*	*45*	*60*	*75*	*90*
Wear $[mg/kg]$	*5.5*	*5.7*	*7.2*	*7.4*	*4.5*	*2.1*	*2.8*	*3*

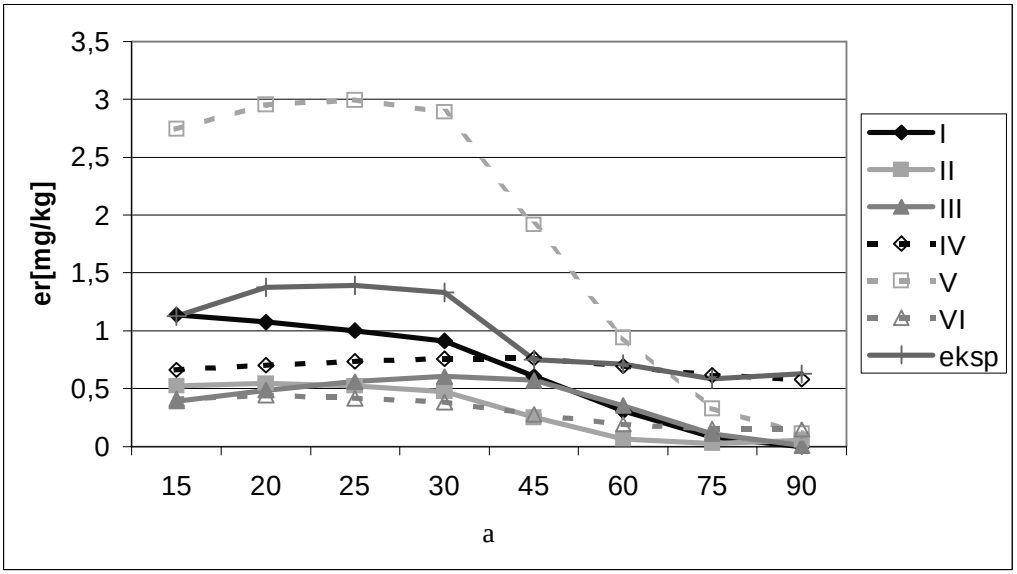

Fig.2. Comparison of calculation results and experimental data for velocity $9.97\,m/s$.

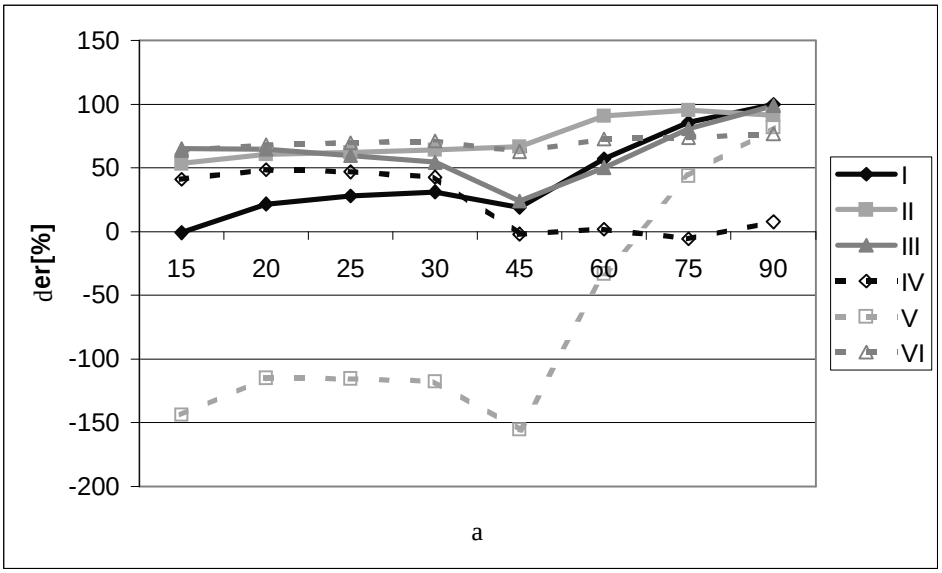

Fig.3. Relative error $\delta_{er}[\%]$ of calculations related to the experimental data for velocity $9.97\,m/s$.

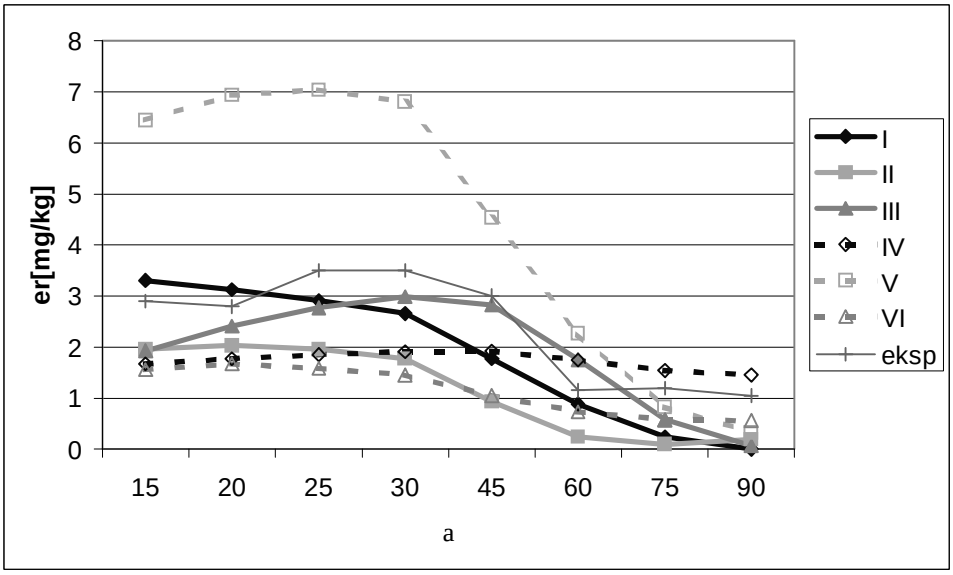

Fig.4. Comparison of calculation results and experimental results for velocity $17\,m/s$.

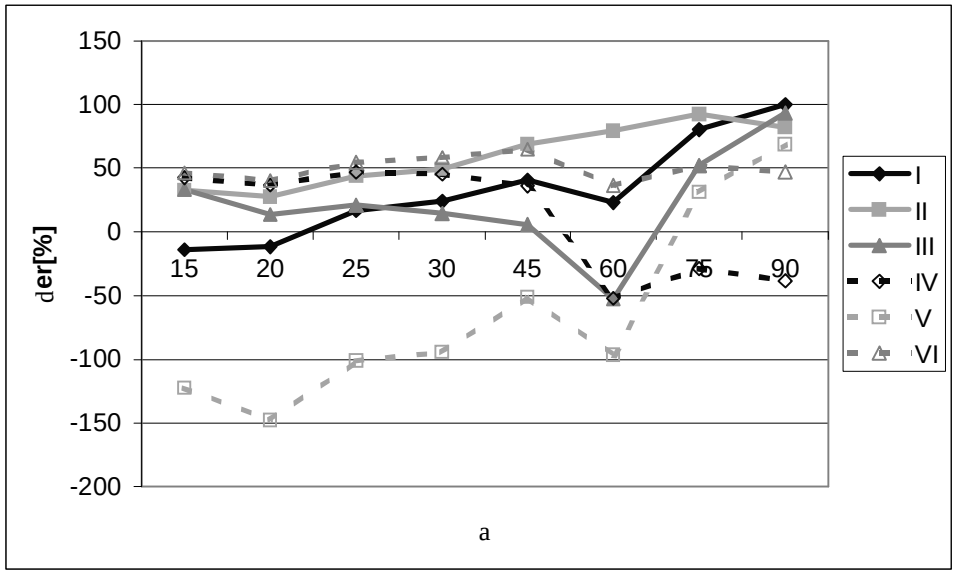

Fig.5. Relative error $\delta_{er}[\%]$ of calculations related to experimental data for velocity $17\,m/s$.

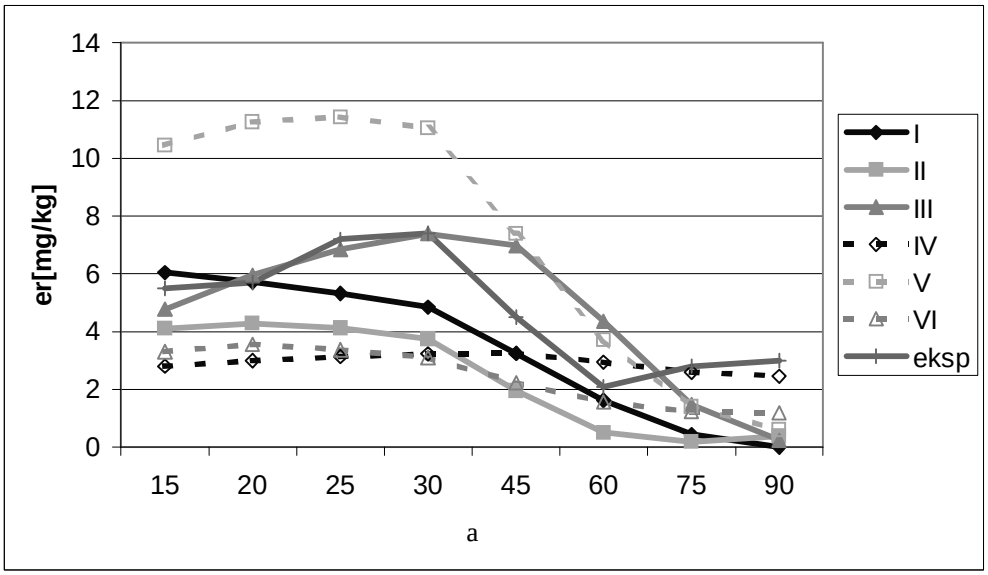

Fig.6. Comparison of calculation results and the experimental data for velocity $23\,m/s$.

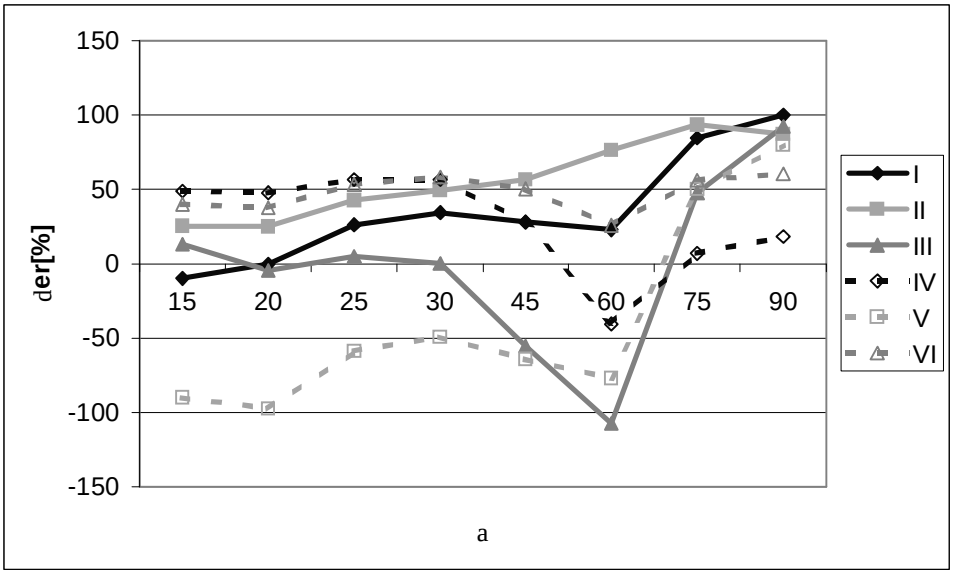

Fig.7. Relative error $\delta_{er}[\%]$ related to experimental data for velocity $23 m/s$.

From a comparison of erosion wear calculated with different methods it appears that the best results are obtained according to Model IV – for the erodent glancing angles above 45^0, Model I – for velocities to $17 m/s$ and the erodent glancing angles to 40^0, and Model III – for velocities greater than $17 m/s$, especially for angles to 45^0.

In order to determine which model is really the best one and expresses wear in a real system, calculations and measurements of the material loss were performed for a dust installation of the BP-1150 boiler. An installation fragment subjected to tests is shown in Fig.8. Detailed measurements were made for a chosen mill installation where a scattering threshold had been provided in order to improve flow conditions before the separator (Fig.9) (Dobrowolski *et al.*, 2004).

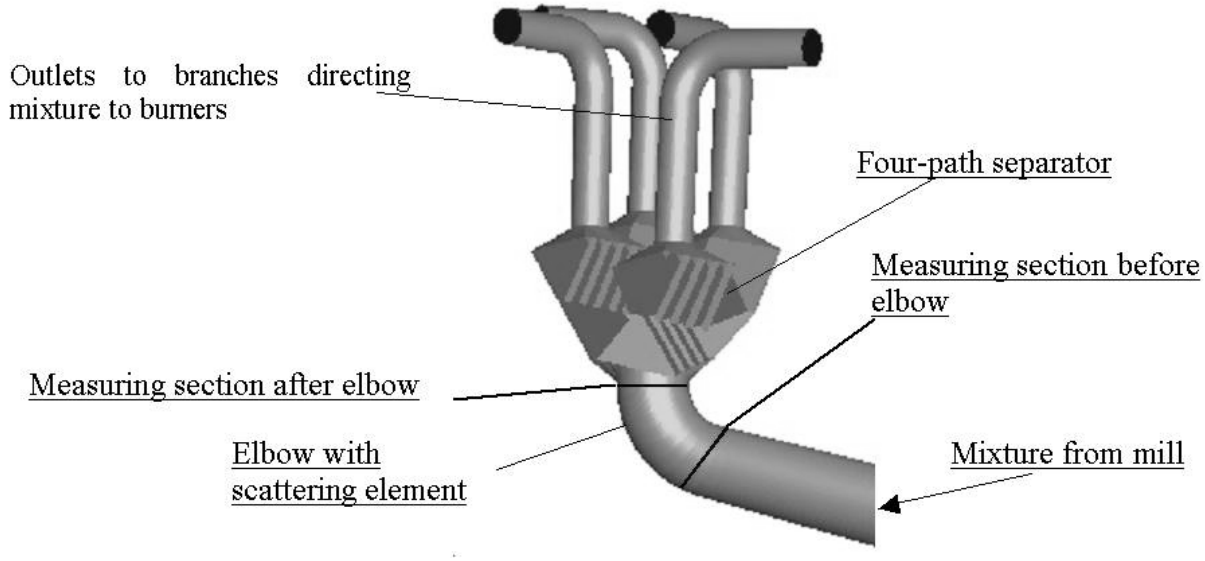

Fig.8. General view of the elbow - four-path separator system.

Figure 9 shows the geometry of the flow system and location of the scattering element, $175mm$ in height, which corresponds to the angle $\phi = 90^0$, and angle β is 13.5^0. Dimensions of the flow system are: $D = 1200mm$, $R = 1180mm$, $lw = 2000mm$.

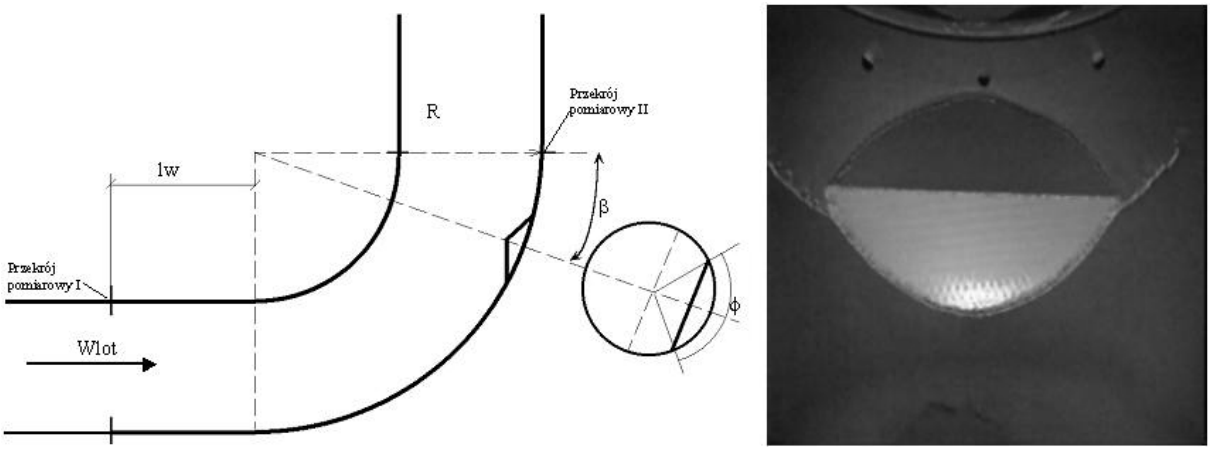

Fig.9. Geometry and view of the flow system with the scattering element.

The position of the scattering element as in Fig.9 causes its higher wear on the wall due to dust action. Wear intensity on this surface makes it possible to determine the dynamics of development of zones with higher erosion wear.

Theoretical foundations presented in the previous chapters were the basis of numerical calculations of erosion wear of the scattering element. The behaviour of the erosion wear models I-VI (Tab.2) under conditions characteristic for the dust system operation and the material pair steel St4s – coal dust was compared.

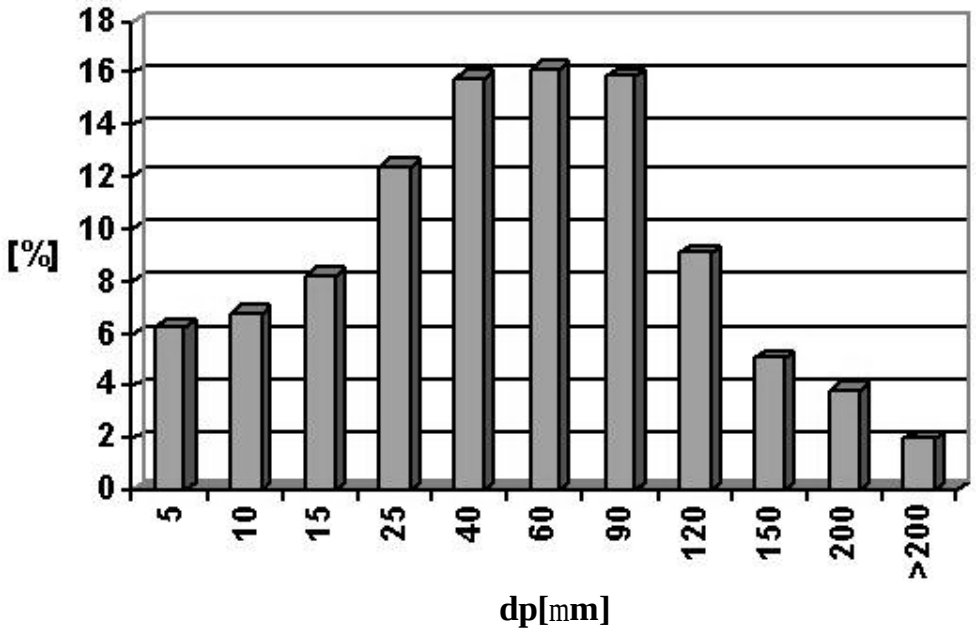

Fig.10. Percentage of particles of particular fractions of coal dust.

In order to calculate the erosion wear rate for the scattering element it was assumed that coal dust contains *7%* of quartz, and further calculations were performed only for particles of quartz as the main component causing erosion wear. The calculations were made for *13* dust diameters: $2.5\mu m$, $5\mu m$, $10\mu m$, $15\mu m$, $25\mu m$, $40\mu m$, $60\mu m$, $90\mu m$, $120\mu m$, $150\mu m$, $200\mu m$, $300\mu m$, and $400\mu m$, assuming fraction distributions resulting from the tests. These data were used for the determination of mass fraction and percentage of particular fractions of the coal dust in the measuring point with the Rosin-Rammler-Sperling method. Figure 10 presents percentage of particular fractions for coal dust. The residuum on the screen $0.2mm$ was *2%*, and on the screen $0.09mm - 20\%$. Calculations of the erosion wear rate were performed with the FLUENT program, completed with our UDF procedure, extending the program possibilities (Wydrych, 2002).

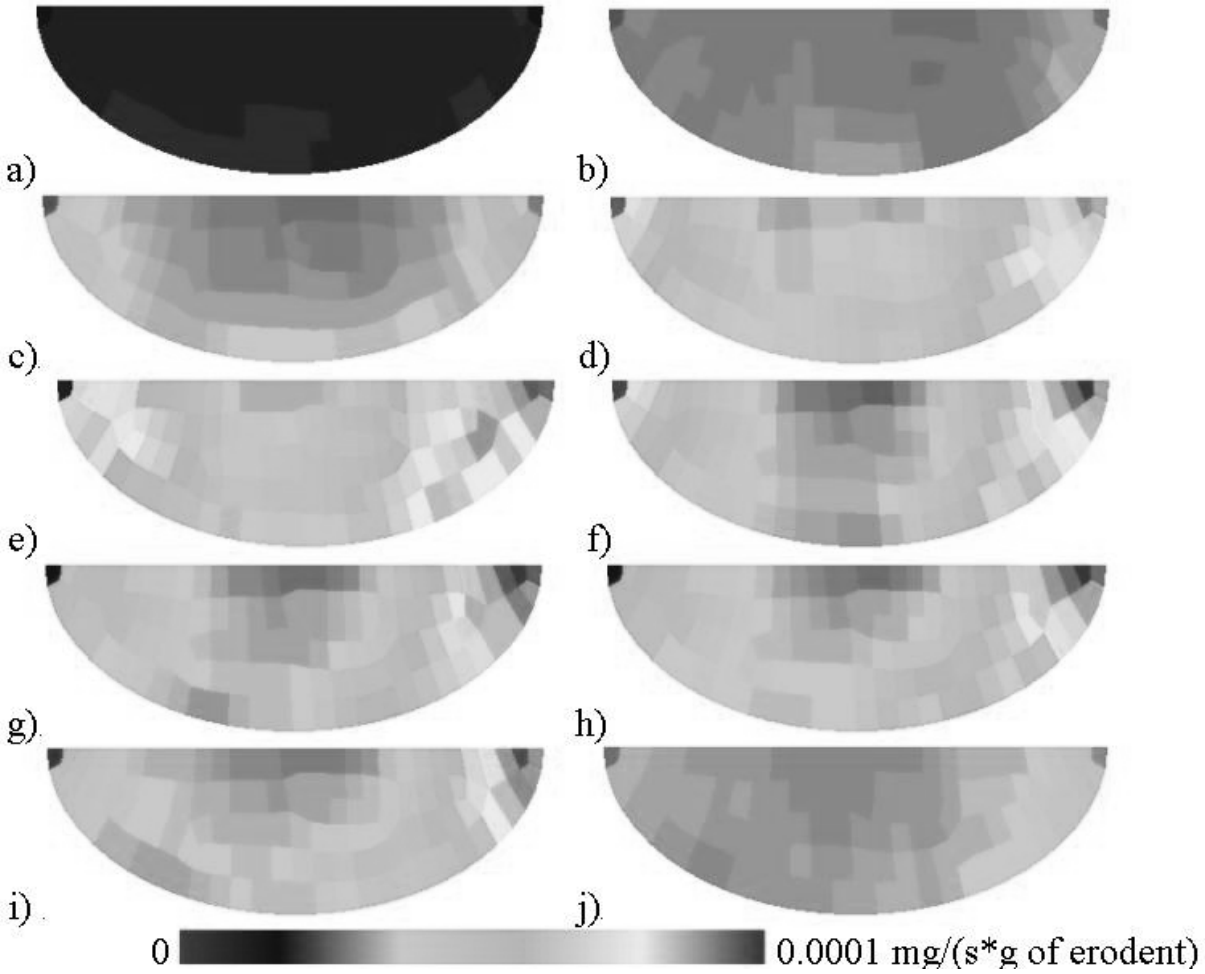

Fig.11. Erosion wear rate of the wall material of the scattering element (in $mg/(s \times g$ of the erodent$)$ for dust particles with diameters: a) $15\mu m$, b) $25\mu m$, c) $40\mu m$, d) $60\mu m$, e) $90\mu m$, f) $120\mu m$, g) $150\mu m$, h) $200\mu m$, i) $300\mu m$, j) $400\mu m$.

Wear rates for the scattering element were calculated for each fraction, and next the total element wear was calculated as a sum of erosion caused by particular fractions.

The data for all the fractions, including periods of different service conditions of the installation, were applied for calculation of the total erosion wear rate for the unitary surface. The total erosion wear rate calculated for the wear model III is shown in Fig.12.

Fig.12. Total erosion wear rate of the wall material of the scattering element in $\mu g/\left(s \times m^2\right)$ for the wear model III.

From the above results it appears that non-uniformity of velocity fields and concentration of the solid fraction of dust mixture strongly influence erosion wear of the scattering element. Similar calculations were performed for other erosion wear models from Tab.2. The results of calculations are presented in Fig.13. For their comparison with the experimental results, they have been shown as erosion wear after *7320h* of service [in g/m^2].

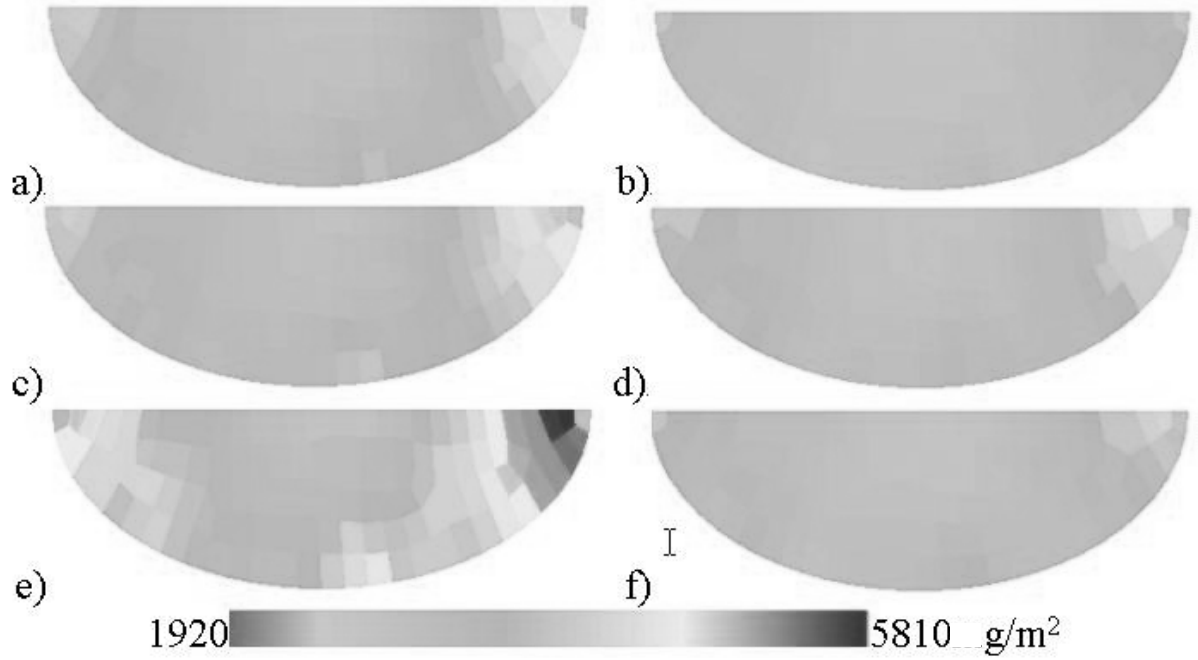

Fig.13. Erosion wear distribution in the wall material of the scattering element expressed in g/m^2 obtained from calculations for the models: a) I, b) II, c) III, d) IV, e) V and f) VI.

From Fig.13 it appears that wear distributions are similar, irrespective of the applied erosion model. Namely, the zone of maximum wear occurs on the right side of the scattering element, and the minimum wear can be observed in the element centre. The observed asymmetry of erosion wear of the surface under consideration is a result of asymmetry of velocity fields and concentration of particles at the inlet section. The total loss of the material of the scattering element determined from numerical calculations was compared with the results of measurements (see Fig.14).

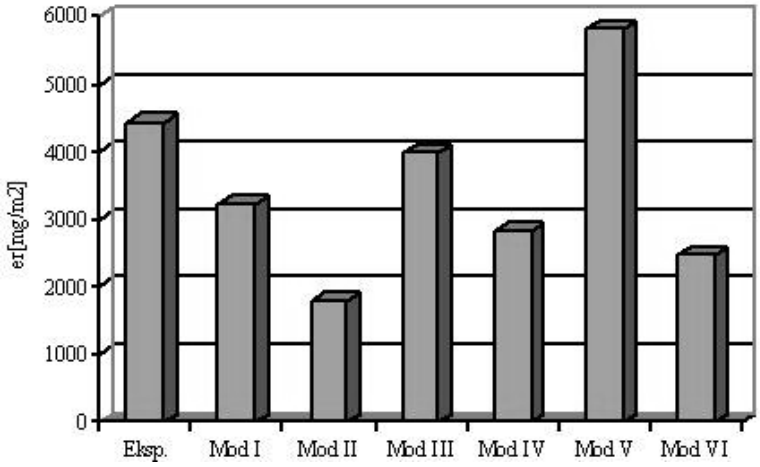

Fig.14. Comparison of erosion wear values obtained according to different models and experimental results.

From the tests carried out for the purpose of this paper it appears that the Model III gives the best results, similar to the results of measurements. Figure 15 shows the erosion wear distribution for the scattering element obtained from numerical calculations with the Model III.

Fig.15. Erosion wear distribution in the wall of the scattering element obtained from numerical calculations after *7320* hours of service.

Figure 16 shows erosion wear distribution for the scattering element obtained from measurements with a ultrasonic thickness gauge of accuracy *0.01mm* (in g/m^2) for service times *3963* and *7320h*.

The results of measurements prove a high asymmetry of distribution of wear zones resulting from non-uniformity of distributions of velocity and concentration of the solid phase behind the coal pulverizer. The results obtained from numerical calculations show a higher wear in all the element area, and this is not proved by tests.

In Fig.16 you can find information about development dynamics and changes of location of wear zones on the scattering element surface. Let us note that the zone of maximum wear is located on the right side of the central part of the plate, and it does not change its position while in service. It means that conditions occurring at the inlet to the system are reproducible.

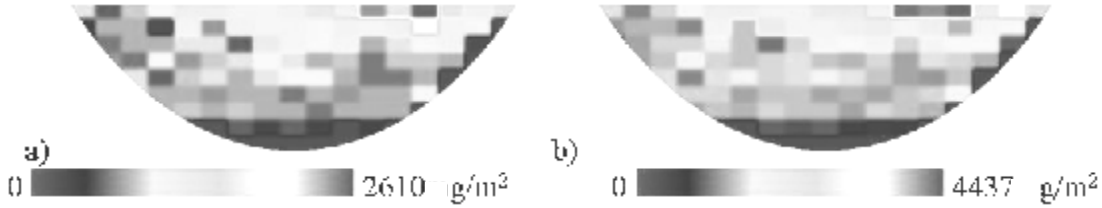

Fig.16. Erosion wear distribution in the wall of the scattering element obtained from experiments for service times a) *3936h* and b) *7320h.*

4. Conclusions

From the tests for a rectangular channel it appears that the results of parametric test and their comparison with the experimental results show a high scatter of the predicted erosion rate. Parameters of the particles when they collide with the wall strongly influence the erosion process. It follows from the parametric test results for different velocities and collision angles realized with our own computer programs. The assumed simplifications and different ranges of applicability of particular models do not allow to state which model should give the correct results under complex flow conditions. Further work on the scattering element in corporated into the dust installation of the boiler BP-1150 allow us to chose the Model III, which gives the best qualitative and quantitative results. Moreover, asymmetry of the erosion loss distribution on the „threshold" surface was found. It results from the asymmetry of the velocity field and particle concentration in the inlet section.

Nomenclature

C_1, C_2, C_μ – empirical constants of turbulence model
d_p – particle diameter, m
f - empirical function
k – kinetic energy of turbulence, m^2/s^2
m_p – mass of particles, kg
p – pressure, Pa
u – gas velocity vector, m/s
u_i – gas velocity vector components in index notation, m/s
u_p – particle velocity vector, m/s
ε – turbulence energy dissipation rate, m^2/s^2
μ – dynamic viscosity, $kg/(ms)$
μ_{ef} – effective viscosity, $kg/(ms)$
μ_t - turbulent viscosity, $kg/(ms)$
ρ – fluid density, m^3/kg
ρ_p – particle density, kg/m^3
σ_k – turbulent Prandtl number
σ_ε – turbulent Schmidt number

References

Bitter J.G.A. (1963): *A study of erosion phenomena*. – Wear, No.6, pp.69-90.

Dobrowolski B., Pospolita J. and Wydrych J. (2004): *Test of improvement in flow conditions before four-path separator for a dust installation of the BP-1150 boiler*. – Inżynieria Chemiczna i Procesowa, vol.25, No.4, pp.2105-2112.

Finnie I. (1960): *Erosion of surfaces by solid particles*. – Wear, No.3, pp.87-103.

FLUENT INC.: *Fluid Dynamics Analysis Package*. – Fluid Dynamic Internationale Inc.

Grant G. and Tabakoff W. (1973): *An experimental investigation of the erosion characteristics of 2024 aluminum alloy*. – Department of Aerospace Enginering Tech. Rep. 73-37, University of Cincinnati.

Jun Yong-Du and Tabakoff W. (1992): *Numerical simulation of a dilute particle flow over tube banks*. – Multiphase Flow in Wells and Pipelines, FED, vol.144, ASME, pp.125-133.

McLaury B., Shirazi S.A., Shadley J.R. and Rybicki E.F. (1996): *Modeling erosion in chokes*. – 1996 Fluids Engineering Division Conference, vol.1, FED, vol.236, ASME, pp.773-781.

Menguturk M. and Sverdrup E.F. (1979): *Calculated tolerance of a large electric utility gas turbine to erosion damage by coal gas ash particles*. – ASTM Spec. Tech. Publ. 664, Philadelphia, PA, pp.193-224.

Sato S., Shimizu A. and Yokomine T. (1995): *Numerical prediction of erosion for suspension flow duct*. – Wear, No.186-187, pp.203-209.

Schuh M.J., Schuler C.A. and Humphrey J.A.C. (1989): *Numerical calculation of particle-laden gas flows past tubes*. – AIChE Journal, vol.35, No.3, pp.466-480.

Wydrych J. (2002): *Aerodynamic coditions of the erosion proces in dust instalations of power boilers*. –Ph.D. Thesis, Opole.

Received: August 1, 2006

Revised: September 5, 2006